JACS
JOURNAL OF THE AMERICAN CHEMICAL SOCIETY
Communication
pubs.acs.org/JACS

Facet-Selective Growth on Nanowires Yields Multi-Component Nanostructures and Photonic Devices

Thomas J. Kempa,[†] Sun-Kyung Kim,[†,§] Robert W. Day,[†] Hong-Gyu Park,*[,∥] Daniel G. Nocera,*[,†] and Charles M. Lieber*[,†,‡]

[†]Department of Chemistry and Chemical Biology and [‡]School of Engineering and Applied Sciences, Harvard University, Cambridge, Massachusetts 02138, United States

[§]Department of Applied Physics, Kyung Hee University, Gyeonggi-do 446-701, Republic of Korea

[∥]Department of Physics, Korea University, Seoul 136-701, Republic of Korea

Supporting Information

ABSTRACT: Enhanced synthetic control of the morphology, crystal structure, and composition of nanostructures can drive advances in nanoscale devices. Axial and radial semiconductor nanowires are examples of nanostructures with one and two structural degrees of freedom, respectively, and their synthetically tuned and modulated properties have led to advances in nanotransistor, nanophotonic, and thermoelectric devices. Similarly, developing methods that allow for synthetic control of greater than two degrees of freedom could enable new opportunities for functional nanostructures. Here we demonstrate the first regioselective nanowire shell synthesis in studies of Ge and Si growth on faceted Si nanowire surfaces. The selectively deposited Ge is crystalline, and its facet position can be synthetically controlled *in situ*. We use this synthesis to prepare electrically addressable nanocavities into which solution soluble species such as Au nanoparticles can be incorporated. The method furnishes multicomponent nanostructures with unique photonic properties and presents a more sophisticated nanodevice platform for future applications in catalysis and photodetection.

Semiconductor nanowires (NWs) represent a diverse class of nanomaterials whose synthetically tunable structural, electronic, and optical properties[1−3] have enabled active nanodevices including high-performance field-effect transistors,[4] ultrasensitive biological probes,[5−7] and solar cells and photonic devices with tunable optical spectra.[8−12] NWs can be classified according to the number of degrees of freedom (DoF) they possess, which represent fundamental physical coordinates along which their structure can be manipulated. Axial and radial (core/shell) modulated NWs have 1 and 2 DoF, respectively, and have been extensively studied and characterized.[2,13−19] Nevertheless, the properties of nanostructures possessing greater complexity and anisotropy have not been determined.

A nanostructure with 3 DoF and higher can be realized by breaking the rotational symmetry of conventional radial shell growth (Figure 1A). A high-resolution scanning electron micrograph (SEM) of a faceted core/shell Si NW (Figure 1B) reveals well-defined surfaces that were previously indexed[9] as {111}, {011}, and {113}. NWs with this same morphology and set of surface facets serve as the faceted templates from which all subsequent nanostructures in this study are grown. Following chemical vapor deposition (CVD) synthesis of the SiNW templates,[9] introduction of GeH_4 and H_2 at lower temperature and pressure into the same reactor (Supporting Information) yields a new product featuring selective material deposition on the {111} and {011} Si surface facets (Figure 1B). Energy dispersive X-ray spectroscopy (EDS) performed on the nanostructure (Figure 1C) confirms the elemental identity of the deposited material as Ge and reveals that facet selectivity is preserved along the length of the nanostructure. A planview transmission electron micrograph (TEM) of the anisotropic Si−Ge nanostructure (Figure 1D) reveals mesas with a uniform dark contrast corresponding to Ge. The Ge appears smooth and ordered and extends uniformly along the length of the {011} facet to which it is bound. Notably, these results differ significantly from the disordered, island morphologies that typify Stranski−Krastanov growth of Ge on planar and nanoscale Si surfaces.[20−23]

We performed syntheses using different Si templates, temperatures, and gas-phase species to determine their role in growth of Si−Ge (heteroepitaxial) and Si−Si (homoepitaxial) nanostructures with distinct anisotropies. After performing each synthesis for 5 min (Figure 2A, Figures S1 and S2), we prepared 40 nm thick cross sections of the synthesized nanostructures and analyzed their morphology by bright-field TEM (Figure 2B, Figures S1 and S2).

TEM analysis of a nanostructure synthesized at 330 °C with GeH_4 and H_2 reveals dark contrast corresponding to Ge that has selectively grown on the {111} and {011} surfaces of the template (Figure 2, structure **1**). No dark contrast is visible on the {113} Si surfaces, thus reinforcing our previous contention of high selectivity for this Ge growth (Figure 1). Some variation in the Si morphology reflects both natural dispersion and TEM sample preparation (Figure S3 and the Supporting Information). From TEM measurements and Ge growth time, we estimate the growth rates of Ge on {011} and {111} surfaces to be 2 and 1 nm/min, respectively. Repeating this synthesis in the

Received: October 29, 2013
Published: November 26, 2013

ACS Publications © 2013 American Chemical Society

dx.doi.org/10.1021/ja411050r | J. Am. Chem. Soc. 2013, 135, 18354−18357

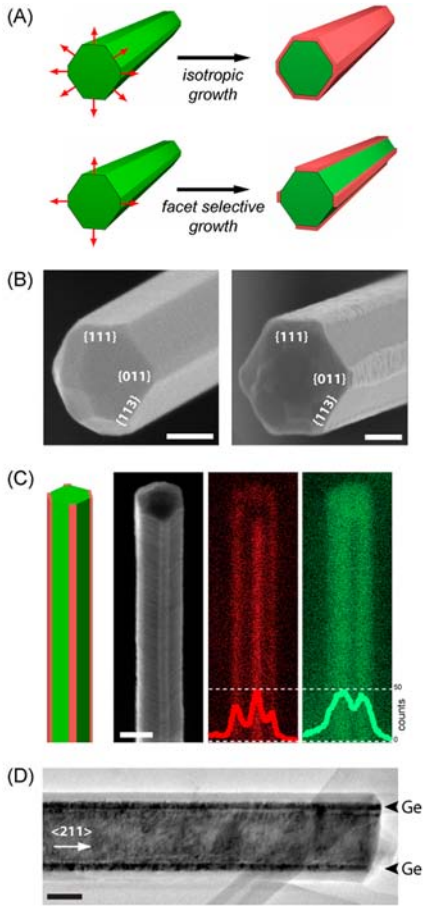

Figure 1. (A) Schematics depicting isotropic (top) versus anisotropic (bottom) growth of Ge (red) on a faceted Si template (green). (B) SEM of a faceted Si template (left) and of a nanostructure (right) after selective deposition of 10 nm of Ge (lighter contrast) on Si{111} and {011} surfaces. Images are oriented with {111} surfaces on top and bottom. Scale bars, 100 nm. (C) Schematic and SEM of a single nanostructure. Ge (red) and Si (green) EDS elemental maps of the same nanostructure and line profiles extracted from signal counts along the *x*-axis of the images. Images are oriented with the {011} surface facing the reader. Scale bar, 200 nm. (D) Bright-field planview TEM of a nanostructure. Scale bar, 100 nm.

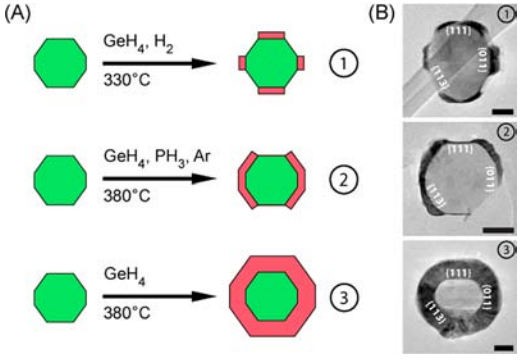

Figure 2. (A) Schematics summarizing three syntheses conducted to explore control of facet selective growth of Ge (red) on a faceted Si template (green). (B) Bright-field TEMs of 40 nm thick cross sections of nanostructures **1**–**3** prepared according to the syntheses outlined in part A. Images are oriented with {111} surfaces on top and bottom. Scale bars, 50 nm.

presence of the faceted Si template coated with a 3 nm thick amorphous Si layer yields a thin isotropic Ge shell (Figure S1). Interestingly, growth at 650 °C with SiH_4 and H_2 leads to selective Si growth on the {111} surfaces of the Si template (Figure S2). This result is in contradistinction to the isotropic nanocrystalline Si shell[24] observed when this synthesis is performed on an axial Si NW without well-defined surface facets. Together, these results demonstrate that the surface properties of the template play a vital role in enabling and controlling facet selective growth.

To determine whether Ge can be selectively grown on other facets, we examined syntheses at higher temperature and with various gas-phase precursors. TEM analysis of a nanostructure synthesized at 380 °C with GeH_4, PH_3, and Ar reveals (Figure 2, structure **2**) estimated Ge growth rates on the {113}, {011}, and {111} surfaces of 3.0, 1.6, and 0.3 nm/min, respectively. In structure **2**, a ×10 faster growth rate of Ge on {113} versus {111} is a striking reversal of the observed growth trend on these surfaces for structure **1**. We determined that Ar alone enhances growth of Ge on {113} versus {111}, whereas PH_3 improves selectivity by suppressing Ge growth on the {111} surface, likely through passivation of Si surface sites with adsorbed phosphine or phosphine-derived species.[10,25] Finally, TEM analysis of a nanostructure synthesized at 380 °C with GeH_4 and no other gas-phase species reveals (Figure 2, structure **3**) an isotropic Ge shell and an estimated growth rate for this shell of 10 nm/min. This result confirms the importance of gas-phase species in mediating facet selective growth of Ge at higher temperatures. The yields of structures **1**–**3** determined from random sampling are in the range 70–90%. In summary, these results represent the first gas-phase facet selective growth of Ge and Si on Si nanowire surfaces and establish that their facet position can be synthetically controlled *in situ* to elaborate unique nanostructures with higher anisotropy.

To explore more complex and opto-electronically active nanostructures, we encapsulated nanoscale Ge regions within a Si p–n interface. The targeted architecture includes a faceted template with p-type and intrinsic Si shells, facet selective grown Ge, and finally a conformal shell of n-type Si (Figure 3A and the Supporting Information). Notably, all synthetic steps were carried out in a continuous sequence in a single reactor for this complex structure. Bright-field TEM (Figure 3B) and EDS (Figure 3C, Figure S4) elemental mapping of the nanostructure cross section verify that Ge was selectively embedded within the nanostructure while preserving the radial Si p–n junction. High-resolution TEM analysis of a region of the cross section near the Si{111} interface (Figure 3D) reveals several important features. First, crystal lattice fringes proceed through the intrinsic Si/Ge/*n*-type Si regions of interest and terminate at the amorphous SiO_x layer passivating the nanostructure. Second, two-dimensional Fourier transforms (Figure 3D) of lattice resolved TEM images from the intrinsic Si and Ge regions show well resolved spots that are consistent with the [211] zone axis of the cubic crystal lattice.[26] Third, the sharp contrast changes visible in bright-field (Figure 3D) and dark-field TEM (Figure S4, inset) depict the abrupt interfaces formed between Si and Ge. In addition, high resolution TEM of a region of the cross section near the Si{113} interface (Figure 3E) reveals an apparently clean intrinsic Si/n-type Si interface. Together, these results verify that the facet selective growth of Ge and subsequent conformal growth of n-type Si are

dx.doi.org/10.1021/ja411050r | J. Am. Chem. Soc. 2013, 135, 18354–18357

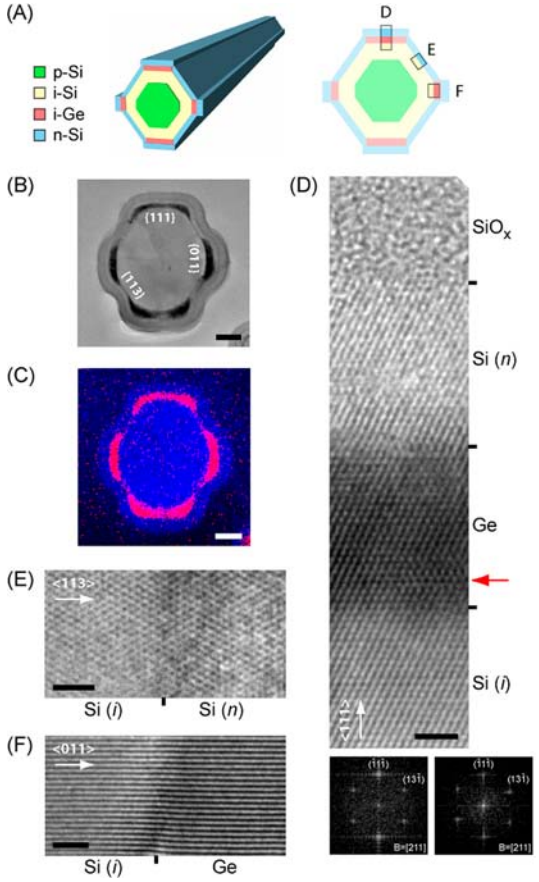

Figure 3. (A) Schematic (left) depicting a complex nanostructure with Ge regions selectively embedded within a p−i−n junction. Schematic (right) of the nanostructure cross section with labels D, E, and F corresponding to the figure panels where these interfaces are presented in detail. (B) Bright-field TEM of a 40 nm thick cross section of the active nanostructure. The image is oriented with {111} surfaces on top and bottom. Scale bar, 50 nm. (C) EDS elemental map of the section shown in part B revealing Ge (red) embedded in Si (blue). Scale bar, 50 nm. (D) High-resolution TEM of the intrinsic Si/Ge/n-type Si region near the {111} interface within the nanostructure. The {111} plane lies parallel to the *x*-axis of the image. Two-dimensional FFTs of lattice-resolved TEMs of intrinsic Si (left) and Ge (right) regions. The cross section is perpendicular to the nanostructure [211] zone axis. The red arrow indicates the site of misfit dislocation. Scale bar, 2 nm. (E) High-resolution TEM of the intrinsic Si/n-type Si region near the {113} interface within the nanostructure. The {113} plane lies parallel to the *y*-axis of the image. Scale bar, 2 nm. (F) High-resolution TEM of the intrinsic Si/Ge region near the {011} interface within the nanostructure. The {011} plane lies parallel to the *y*-axis of the image. Scale bar, 2 nm.

crystalline and that clean, atomically sharp interfaces can be designed and realized in these complex nanostructures.

High-resolution TEM analysis of a region of the cross section near the Si{011} interface (Figure 3F and Figure S5) reveals several unique features. First, Si{111} lattice fringes progress across the intrinsic Si/Ge junction and are distorted near the edge of the Ge mesa where the Si{011} and {113} surfaces meet (Figure 3F). Second, a TEM spanning the full width of this region (Figure S5) shows a region of crystalline Ge that is 15 nm wide. Growth of planar Ge films on Si typically proceeds by the Stranski−Krastanov mechanism.[20] An initial stage of epitaxial growth for thicknesses <5 nm[20] is followed by a disordered, three-dimensional (island) phase as strain energy increases due to the 4.2% Ge−Si lattice mismatch. Notably, our results demonstrate epitaxial Ge growth over greater thicknesses and suggest this is due to homogeneous relaxation of compressive strain[27,28] in the {011} plane, facilitated by the absence of crowding species on the adjacent {113} surface. Likewise, epitaxial growth of Ge persists for growth in the ⟨111⟩ direction and shows evidence of the formation of misfit dislocations[27,28] ∼4 epilayers distant from the intrinsic Si/Ge interface (Figure 3D). The properties of the localized Si−Ge heterostructure regions and/or the role of Ge as a sensitizer within the nanostructure will be of future interest.

As a first step toward examining the optoelectronic properties of nanostructures with newly accessible anisotropies, we prepared a novel nanostructure with functional nanocavities. Specifically, hydrogen peroxide was used to etch Ge selectively and thus convert the nanostructure synthesized in Figure 3 to one with controlled nanocavities embedded within the p−n junction (Figure 4A and the Supporting Information). SEM and TEM analyses (Figure 4B) verify that well-defined nanoscale cavities were etched in place of the Ge and that they extend uniformly along the lengths of the facet, where longitudinal etch distance is a function of the H_2O_2 etch time.

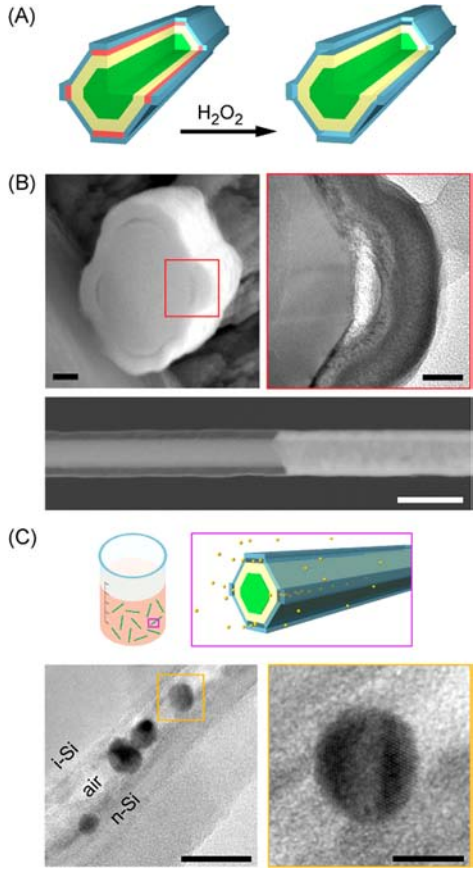

Figure 4. (A) Schematic demonstrating selective etching of Ge in H_2O_2 to form nanocavities. (B) SEM (left, scale bar, 50 nm) of the end of an etched nanostructure; high-resolution TEM (right, scale bar, 20 nm) of a cross section near the {011} interface. Planview SEM (bottom, scale bar, 500 nm) of an etched nanostructure. (C) Schematic showing immersion of etched nanostructure in Au colloid solution. TEM image (left, scale bar, 20 nm) showing four Au nanoparticles infiltrated into the nanostructure cavity. High-resolution TEM image (right, scale bar, 5 nm) showing a magnified view of a 7 nm Au nanoparticle.

dx.doi.org/10.1021/ja411050r | J. Am. Chem. Soc. 2013, 135, 18354−18357

Next, we fabricated single nanodevices with either a 10 or 20 nm wide nanocavity. Experimental and simulated external quantum efficiency (EQE) spectra (Figure S6) obtained for the single nanodevices highlight several new features. An absorption centered at 500 nm (Figure S6A, peak 1) increases in amplitude as nanocavity size is enlarged from 10 to 20 nm. This enhanced absorption is well reproduced by simulation (Figure S6B, peak 1) and attributed to an increase in optical feedback (Figure S6C) due to change of refractive index[29,30] within the porous nanostructure. In addition, a very weak absorption at 625 nm blue shifts by 40 nm and its amplitude increases by a factor of 2.0 as nanocavity size is increased by 10 nm (Figure S6A, peak 2). Simulation shows reasonable agreement with this trend, predicting a 30 nm blue shift and 2-fold increase in amplitude for the same nanocavity size change (Figure S6B, peak 2). Analysis of simulated absorption mode profiles ascribes the wavelength shift to mode-pulling (Figure S6C) toward the lower refractive index air-filled nanocavity.[29,30] Notably, additional simulation results indicate that the spectral properties of these nanostructures can be significantly altered through subtle modification of the size and position of the internal nanocavities.

Nanoscale species may be delivered into the NW nanocavities. Immersion of the nanoporous structure in a 5 nm Au colloid solution led to infiltration of Au nanoparticles into the nanocavities (Figure 4C). A planview TEM of the nanostructure following immersion shows four Au nanoparticles trapped within a nanocavity (Figure 4C) that is encapsulated by intrinsic and n-type Si. This approach should be general for both metal and semiconductor nanoparticles as well as molecular dyes, thus opening up a new avenue for study of photosensitization and catalysis in unique electrically addressable nanocavities. A nanostructure−catalyst framework presents a unique nanoporous scaffold within which to self-assemble catalysts; such a motif is appealing for the assembly of catalysts employed in energy conversion.[31] In addition, we expect our approach can accomplish facet selective synthesis of III/V or II/VI semiconductor NW materials, and nanoporous NW structures of these materials, that will be interesting targets of future study.

■ ASSOCIATED CONTENT

Supporting Information

Detailed description of synthetic methods, sample preparation, and device fabrication; additional figures; and additional references. This material is available free of charge via the Internet at http://pubs.acs.org.

■ AUTHOR INFORMATION

Corresponding Authors

hgpark@korea.ac.kr
dnocera@fas.harvard.edu
cml@cmliris.harvard.edu

Notes

The authors declare no competing financial interest.

■ ACKNOWLEDGMENTS

T.J.K. acknowledges a National Science Foundation Graduate Research Fellowship. C.M.L. acknowledges support of this research from a DOD NSSEFF (N00244-09-1-0078) Award. D.G.N. acknowledges support of NSF CCI (CHE-1305124). H.-G.P. acknowledges a MSIP grant (2009-0081565) from the National Research Foundation of Korea.

■ REFERENCES

(1) Lu, W.; Lieber, C. M. *Nat. Mater.* **2007**, *6*, 841−850.
(2) Lu, W.; Lieber, C. M. *J. Phys. D: Appl. Phys.* **2006**, *39*, 387−406.
(3) Xia, Y.; Yang, P.; Sun, Y.; Wu, Y.; Mayers, B.; Gates, B.; Yin, Y.; Kim, F.; Yan, H. *Adv. Mater.* **2003**, *15*, 353−389.
(4) Xiang, J.; Lu, W.; Hu, Y.; Wu, Y.; Yan, H.; Lieber, C. M. *Nature* **2006**, *441*, 489−493.
(5) Patolsky, F.; Timko, B. P.; Zheng, G.; Lieber, C. M. *MRS Bull.* **2007**, *32*, 142−149.
(6) Tian, B.; Cohen-Karni, T.; Qing, Q.; Duan, X.; Xie, P.; Lieber, C. M. *Science* **2010**, *329*, 830−834.
(7) Cohen-Karni, T.; Timko, B. P.; Weiss, L. E.; Lieber, C. M. *Proc. Natl. Acad. Sci. U.S.A.* **2009**, *106*, 7309−7313.
(8) Tian, B.; Kempa, T. J.; Lieber, C. M. *Chem. Soc. Rev.* **2009**, *38*, 16−24.
(9) Kempa, T. J.; Cahoon, J. F.; Kim, S.-K.; Day, R. W.; Bell, D. C.; Park, H.-G.; Lieber, C. M. *Proc. Natl. Acad. Sci. U.S.A.* **2012**, *109*, 1407−1412.
(10) Kim, S.-K.; Day, R. W.; Cahoon, J. F.; Kempa, T. J.; Song, K.-Y.; Park, H.-G.; Lieber, C. M. *Nano Lett.* **2012**, *12*, 4971−4976.
(11) Cao, L.; White, J. S.; Park, J.-S.; Schuller, J. A.; Clemens, B. M.; Brongersma, M. L. *Nat. Mater.* **2009**, *8*, 643−647.
(12) Kelzenberg, M. D.; Turner-Evans, D. B.; Kayes, B. M.; Filler, M. A.; Putnam, M. C.; Lewis, N. S.; Atwater, H. A. *Nano Lett.* **2008**, *8*, 710−714.
(13) Kempa, T. J.; Tian, B.; Kim, D. R.; Hu, J.; Zheng, X.; Lieber, C. M. *Nano Lett.* **2008**, *8*, 3456−3460.
(14) Tian, B.; Xie, P.; Kempa, T. J.; Bell, D. C.; Lieber, C. M. *Nat. Nanotechnol.* **2009**, *4*, 824−829.
(15) Qian, F.; Li, Y.; Gradecak, S.; Park, H.-G.; Dong, Y.; Ding, Y.; Wang, Z. L.; Lieber, C. M. *Nat. Mater.* **2008**, *7*, 701−706.
(16) Caroff, P.; Dick, K. A.; Johansson, J.; Messing, M. E.; Deppert, K.; Samuelson, L. *Nat. Nanotechnol.* **2009**, *4*, 50−55.
(17) Wacaser, B. A.; Dick, K. A.; Johansson, J.; Borgstrom, M. T.; Deppert, K.; Samuelson, L. *Adv. Mater.* **2009**, *21*, 153−165.
(18) Schmidt, V.; Wittemann, J. V.; Gosele, U. *Chem. Rev.* **2010**, *110*, 361−388.
(19) Kodambaka, S.; Tersoff, J.; Reuter, M. C.; Ross, F. M. *Science* **2007**, *316*, 729−732.
(20) Eaglesham, D. J.; Cerullo, M. *Phys. Rev. Lett.* **1990**, *64*, 1943−1946.
(21) Kwon, S.; Chen, Z. C. Y.; Kim, J.-H.; Xiang, J. *Nano Lett.* **2012**, *12*, 4757−4762.
(22) Pan, L.; Lew, K.-K.; Redwing, J. M.; Dickey, E. C. *Nano Lett.* **2005**, *5*, 1081−1085.
(23) Ben-Ishai, M.; Patolsky, F. *Adv. Mater.* **2010**, *22*, 902−906.
(24) Tian, B.; Zheng, X.; Kempa, T. J.; Fang, Y.; Yu, N.; Yu, G.; Huang, J.; Lieber, C. M. *Nature* **2007**, *449*, 885−890.
(25) Cho, B.; Bareno, J.; Foo, Y. L.; Hong, S.; Spila, T.; Petrov, I.; Greene, J. E. *J. Appl. Phys.* **2008**, *103*, 123530:1−10.
(26) Wang, Z. L.; Kang, Z. C. *Functional and smart materials: Structural evolution and structure analysis*; Plenum Press: New York, 1998.
(27) Mullner, P.; Gao, H.; Ozkan, C. S. *Philos. Mag. A* **1997**, *75*, 925−938.
(28) Luth, H. *Solid Surfaces, Interfaces, and Thin Films*, 3rd ed.; Springer: New York, 2001.
(29) Hecht, E. *Optics*, 4th ed.; Addison-Wesley: New York, 2002.
(30) Almeida, V. R.; Xu, Q.; Barrios, C. A.; Lipson, M. *Opt. Lett.* **2004**, *29*, 1209−1211.
(31) Surendranath, Y.; Lutterman, D. A.; Liu, Y.; Nocera, D. G. *J. Am. Chem. Soc.* **2012**, *134*, 6326−6336.